Numerical Simulations of the Partially-ionized Gas in a 100-A LaB_6 Hollow Cathode

IEPC-2013-142

Presented at the 33rd International Electric Propulsion Conference,
The George Washington University • Washington, D.C. • USA
October 6 – 10, 2013

Ioannis G. Mikellides,[*] Dan M. Goebel,[†] Benjamin A. Jorns,[‡] James E. Polk[§] and Pablo Guerrero[**]
Jet Propulsion Laboratory, California Institute of Technology, Pasadena, CA, 91109

Numerical simulations of a hollow cathode with a LaB_6 emitter operating at 100 A have been performed for the first time using the 2-D Orificed Cathode (OrCa2D) code. Results for a variety of plasma properties are presented and compared with laboratory measurements. The large size of the device permits peak electron number densities in the cathode interior that are lower than those established in the NSTAR hollow cathode, which operates at a 7.3× lower discharge current and 3.2× lower mass flow rate. The maximum electron current density also is lower in the LaB_6 cathode, by 4.2×, due to the larger orifice size. Simulations and direct measurements show that at 12 sccm of xenon flow the peak emitter temperature is in the range of 1630-1666 ^{o}C. It is also found that the conditions for the excitement of current-driven streaming instabilities and ion-acoustic turbulence (IAT) are satisfied in this cathode, similarly to what was found in the past in its smaller counterparts like the NSTAR cathode. Based on numerical simulations, it has long been argued that these instabilities may be responsible for the anomalously large ion energies that have been measured in these discharges as well as for the enhancement of the plasma resistivity. Direct measurements of the turbulent spectra and confirmation of the presence of IAT in this cathode are presented for the first time in a companion paper. Interpolation of the measured anomalous collision frequency based on slightly different operating conditions than the one in the numerical simulations suggests good agreement with the computed values.

I. Introduction

As a first step to a long-term vision of human and robotic exploration missions NASA is considering an Asteroid Retrieval Mission (ARM). The performance capability of high-power (20-100 kW) Hall thrusters (T>1 N, I_{sp}=2000-3000 s) makes them the leading Solar Electric Propulsion (SEP) technology for this mission. After the breakthrough advances in their throughput capability made in the last few years [1, 2], the last known major life-limiting mechanism that remains unsolved in high-power Hall thrusters is erosion of the keeper electrode in the hollow cathode. Through a competitive internal solicitation in 2012, the Jet Propulsion Laboratory (JPL) awarded a 2-yr Research & Technology Development (R&TD) proposal to (1) better understand the source(s) that lead to erosion of the keeper and (2) to eliminate it as a failure mechanism.

[*] Principal Engineer, Electric Propulsion Group, Ioannis.G.Mikellides@jpl.nasa.gov.
[†] Senior Research Scientist, Thermal and Propulsion Engineering Section, Dan.M.Goebel@jpl.nasa.gov.
[‡‡] Associate Engineer, Electric Propulsion Group, Benjamin.A.Jorns@jpl.nasa.gov.
[§] Principal Engineer, Propulsion, Thermal, & Materials Systems, James.E.Polk@jpl.nasa.gov.
[**] JPL Affiliate, Electric Propulsion Group, p.guerrero.eng@gmail.com or pguerrer@caltech.edu.

High-power Hall thrusters will require cathodes that operate at discharge currents in the range of 50-250 A. Operation at the high end of this range is more than one order of magnitude higher than state-of-the-art cathodes, such as the ones flown on Deep-Space 1 and DAWN. Moreover, their life requirement for human exploration missions would significantly exceed the present capability. For example, the In-Space Propulsion Project, Game Changing Development (GCD) Program at NASA is pursuing 20-50 kW SEP technologies aimed at >200-kW spacecraft for space tug operations, crewed space exploration to Near Earth Objects and cargo transport missions. These missions would require 50-200 A cathodes with life capability that greatly exceeds 15,000 h (1.7 yr). GCD plans also to pursue advanced EP technologies at the 100-kW level aimed at MW-class missions for human exploration in the longer term. These technologies may require >500 A cathodes with similar life requirements. ARMs, like the ones proposed to NASA by the Keck Institute for Space Studies (KISS) team [3], would require >40-kW Hall thrusters for large asteroids with at least 30,000 h of life for each thruster. For these large-asteroid retrieval missions cathodes operating at >50 A will be needed.

In contrast to their counterparts at the lower current levels (<20 A), cathode operation at >100 A is relatively unexplored. Consequently, the required life of the keeper at current levels relevant to the abovementioned missions has never been demonstrated. Hollow cathodes have been operated at discharge currents of the order of 100 A for only a few hundred hours. One of the longest wear tests was performed at JPL in 1988 during which an argon-fed cathode was operated for about 1000 h at 100 A. The cathode sustained significant damage and the test had to be terminated due to severe component erosion [4]. It became widely known after this and similar other tests performed at Colorado State University that the cause of keeper erosion is material bombardment by high-energy ions. However, though several hypotheses were made, the source of these high-energy ions remained unproven.

In 2005-2008, after the development of the two-dimensional Orifice Cathode (OrCa2D) code [5, 6] and extensive experimental investigations at JPL [7, 8], we proposed that a possible source of high-energy ions is the free energy available to ions from electron-induced oscillations in the discharge [9, 10]. The origin of the proposed mechanism lies in the first (2004) OrCa2D simulations which revealed that the conditions for the excitement of plasma micro-instabilities in the discharge and, possibly anomalous transport, were satisfied near the cathode orifice region [11, 12]. The good agreement obtained between preliminary model predictions (that partially accounted for these wave effects) and the observed keeper erosion profiles was our first evidence that plasma oscillations could indeed be driving the erosion of the keeper. For cathodes operating at <20 A of interest at the time, however, no direct action to suppress the mechanism was necessary because the concentration of high-energy ions was relatively low. Therefore, the life requirement was met simply by replacing the keeper with a material of lower sputtering yield. Nonetheless, foreseeing the future trends to higher currents we also proposed that the addition of neutral gas into the cathode plume could reduce the concentration of high-energy ions because it would damp out plasma oscillations. In recent experimental work, a gas injection mechanism was tested in a Lanthanum hexaboride (LaB_6) cathode in the range of 50-250 A that yielded significant improvements in suppressing high-energy ions. But at >100 A it was found that too many energetic ions continued to persist near the keeper and thus the life requirements for high-power missions (>15,000 h) could not be met; even with external gas injection the maximum life at 250 A is projected to be <2000 h.

The 2-yr R&TD effort proposes to develop a 250-A LaB_6 cathode with keeper life that exceeds 15,000 h, thereby meeting the potential life requirements of human exploration missions with >20-kW Hall thrusters. Because a 15,000-h life test is beyond the scope of this effort, the life will be demonstrated by a combination of numerical simulations, plasma diagnostics and a 500-h wear test at the end of the second year. In this paper we report on progress in the first-year effort which focused on understanding the behavior of the partially-ionized gas under high discharge currents. We present results from numerical simulations of a LaB_6 cathode at 100 A, and compare with measurements of the time-averaged plasma properties. In a companion paper [13] we report on our investigations of the temporal behavior of the plasma in the near-plume region, which include measurements of the wave dispersion and anomalous resistivity. These measurements confirm the presence of IAT in hollow cathode discharges as originally predicted by the early numerical simulations with OrC2D [12].

II. Models and Methods: The 2-D Axisymmetric Orificed Cathode (OrCa2D) Code

All simulations presented herein have been performed with the 2-D axisymmetric code OrCa2D. Development of the code began almost a decade ago and since then it has been used to simulate a variety of hollow cathodes operating under a wide range of conditions [5, 6, 12, 14-16]. Comparisons with several plasma measurements (e.g. [8, 10]) has helped improve both our understanding of driving processes inside these devices as well as the fidelity of the code. In this section we provide some background about the code focusing on recent augmentations that have not been reported in previous publications.

A. General description and code upgrades

The physics models and numerical methods in OrCa2D have been described in detail in previous articles [5, 6, 12, 16] and will only be described briefly here. The model solves the conservation laws for three species present in the partially-ionized gas: electrons, xenon ions and xenon neutrals. It is assumed that only singly-charged ions are present and that the ionized species satisfy quasi-neutrality. All vectors are defined at cell edges and all scalars are defined at cell centers of a structured computational mesh. The system of equations is solved in a time-split manner. Most plasma equations are solved using strongly-implicit methods. The neutral gas continuity and momentum equations, as well as the ion momentum equation are solved explicitly. The numerical approach for the fluid momentum equations uses an upwind finite volume scheme by applying Godunov's [17] 1st-order upwind fluxes across each edge with no flux-limiting.

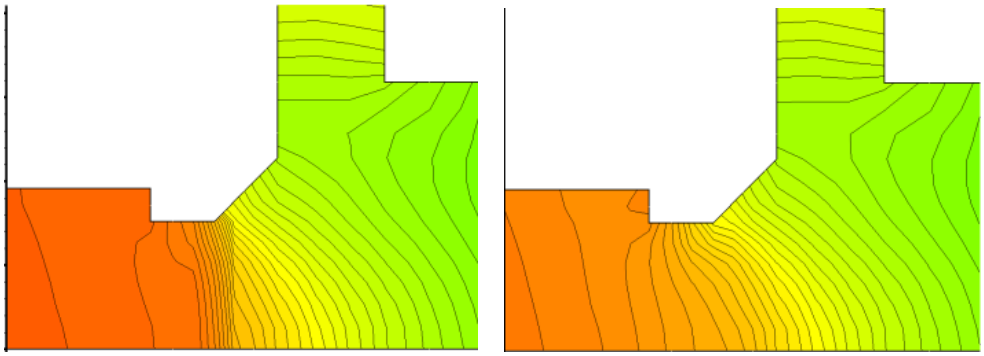

Fig. 1. Contours of computed neutral gas number density in the vicinity of a hollow cathode orifice where transitional flow ($0.1 \lesssim Kn \lesssim 1$) is established. Left: Discontinuous transition based on the previous model of OrCa2D. Right: Smooth transition using a revised model.

Since our last report on simulations with OrCa2D [15], the code has undergone significant improvements. Most notable has been the new capability to perform "cold starts," that is, to execute a simulation from arbitrary initial conditions. Such conditions may include an initial state that emulates the start-up during real operation of the cathode. This new capability overcomes the previous constraint of requiring a pre-existing solution before a new simulation could be performed, which limited considerably the usability of the code. Therefore, OrCa2D can now, in principle, be applied by any user to perform a simulation of any EP hollow cathode. Significant improvements have also been made in the manner in which the collisional to collsionless regions of the neutral gas are coupled. We have shown in the past that the neutral gas inside these devices typically undergoes a transition from low-Knudsen (Kn) number, viscous incompressible flow in the majority of the cathode interior to compressible flow and then to high-Knudsen-number flow in the keeper orifice and plume regions. The violation of the continuum approximation occurs typically in the vicinity of the cathode orifice. Transition flow remains an active area of research today. In OrCa2D we identify *apriory* a "transition boundary" at which the solution method changes from the Navier-Stokes equations to a collisionless approach that assumes neutrals follow straight-line trajectories [18]. The recent improvements in OrCa2D now ensure that this transition

yields smooth change of the mass flux across the cathode orifice from the low-Knudsen number to the high-Knudsen number limit. Contours of the neutral gas density in the orifice region of a hollow cathode using the previous version of the code, showing a discontinuous change of the density across the transition boundary, are illustrated in Fig. 1-left. The new solution showing smooth transition through the orifice is depicted in Fig. 1-right.

OrCa2D now also employs a mesh generator that was developed for the Hall2De code, a 2-D solver of the partially ionized gas in Hall thrusters [19]. The new generator allows for easier and faster development of a computational mesh for a hollow cathode operating with or without an applied magnetic field. The new generator now allows for the simulation of a wider range of hollow cathode geometries, and a mesh generation development time that is at least one order of magnitude less than the previous approach.

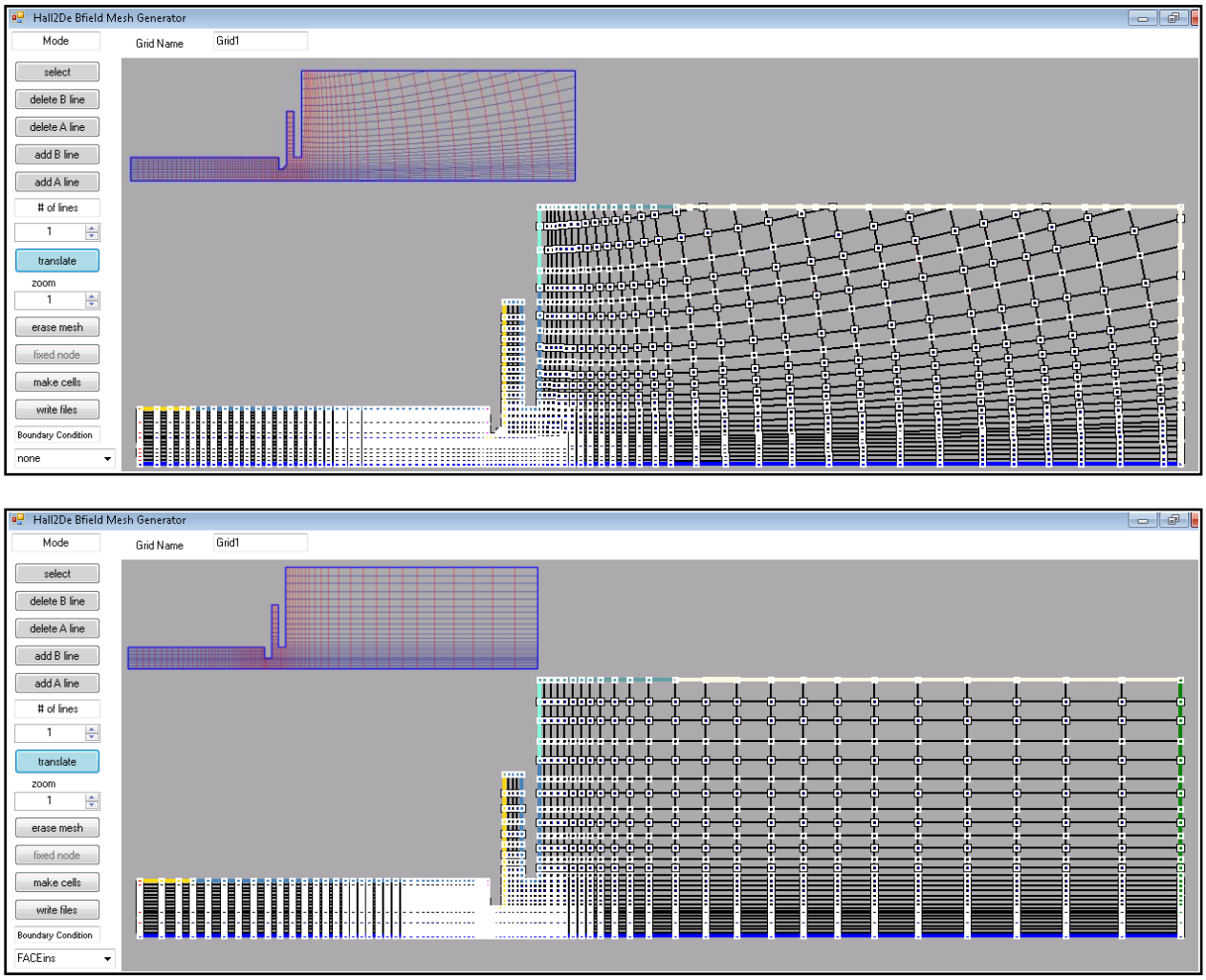

Fig. 2. OrCa2D has been revised to use the mesh generator from the magnetic-field-aligned-mesh Hall thruster code Hall2De [19]. Different colors along the boundary indicate distinct boundary conditions (BC). The generator allows for computations of a much wider range of hollow cathode geometries and applied magnetic field topologies while reducing by at least one order of magnitude the simulation set-up time. Both magnetic-field-aligned (top) and rectilinear meshes (bottom) can be constructed. Because all simulations presented in this paper have been performed in the absence of an applied magnetic field the rectilinear grid (bottom) has been employed.

B. **Governing Equations**

The conservation laws for the partially-ionized gas, Eqs (1)-(8), and related BCs have been presented in detail in previous articles [5, 6, 12, 16] and will only be described briefly here. In the 2-D model, the equations of continuity and momentum for ions (Eqs. (1), (5) and (3) respectively), and the momentum equation for the electrons (Eq. (3)), are solved directly to yield the plasma particle density, n ion and electron current densities $\mathbf{j}_i$ and $\mathbf{j}_e$ respectively. The ion, electron and neutral velocities are denoted by $\mathbf{u}_i$, $\mathbf{u}_e$ and $\mathbf{u}_n$ respectively. The ion/electron pressure and temperature is $p_{i/e}$ and $T_{i/e}$ respectively, and the collision frequencies are denoted by ν. In all previous simulations with OrCa2D the ion inertia terms (LHS terms in Eq. (3)) were neglected. In the present series of simulations we have incorporated these terms to assess their effects on the discharge plasma. This topic is discussed further in Sec. III. The combination of the electron and ion continuity equations yields the current conservation law (Eq. (6)), which is solved for the plasma potential ϕ. The electric field is given by $\mathbf{E}$. The electron temperature is obtained from the electron energy transport equation (Eq. (7)). The energy equation includes thermal diffusion, energy losses due to ionization, where ε_{ip} is the ionization potential of singly-charged ions, and the work done on the electrons by the electric field. The ions and neutrals are assumed to be in thermal equilibrium at temperature T_h and a single equation is employed for the conservation of energy of the heavy species. Terms "Q" in Eqs (7) and (8) represent frictional and thermal heating processes and have been defined in previous articles [5, 16]. In the energy equations $\kappa_{i/e/n}$ denotes the ion/electron/neutral thermal conductivities. The neutral gas density is determined by the neutral gas continuity equation (Eq. (2)), which includes the ionization source term $\dot{n}$. Inside the cathode the neutral gas satisfies the continuum assumption so the fluid momentum equation (Eq. (4)) is solved to yield the neutral gas flux. We have shown in the past that neutral gas viscosity cannot be neglected [16] in most hollow cathodes of interest to EP so the full Navier-stokes equations are in fact solved in the cathode interior, with $\bar{\boldsymbol{\tau}}$ denoting the viscous stress tensor. For the simulation of the rarefied-gas regions, which typically occur downstream of the orifice in EP hollow cathodes, it is customary to implement particle methods such as Direct Monte Carlo Simulation (DSMC) or Particle-in-Cell. In OrCa2D we assume that the gas particles expand freely in straight-line trajectories from a pre-determined boundary, the "transition line," which is chosen in the present simulations to be at the exit of the cylindrical orifice section of the cathode. Beyond this line a collisionless region is assumed for the neutrals. The fundamental assumption in this region is that the gas emanates from surfaces with a positive normal velocity and a thermal spread perpendicular to that surface. Then at large distances from the surface the spread of the perpendicular velocity is reduced due to geometrical selection. The flux of particles is thus only altered by either an ionization event or an encounter with walls. Particles impacting the walls are assumed to return back to the computational region with a thermal speed that is determined based on the local wall temperature.

$$\frac{\partial n}{\partial t} + \nabla \cdot \left(n u_i \right) = \dot{n} \tag{1}$$

$$\frac{\partial n_n}{\partial t} + \nabla \cdot \left(n_n \mathbf{u}_n \right) = -\dot{n} \tag{2}$$

$$\frac{\partial \left(mn\mathbf{u} \right)_i}{\partial t} + \nabla \cdot \left(mn\mathbf{uu} \right)_i = ne\mathbf{E} - \nabla p_i - nm\left[\nu_{ie} \left(\mathbf{u}_i - \mathbf{u}_e \right) + \nu_{in} \left(\mathbf{u}_i - \mathbf{u}_n \right) \right] \tag{3}$$

$$\frac{\partial \left(mn\mathbf{u} \right)_n}{\partial t} + \nabla \cdot \left(mn\mathbf{uu} \right)_n = mn\nu_{in} \left(\mathbf{u}_i - \mathbf{u}_n \right) - \nabla p_n + \nabla \cdot \bar{\boldsymbol{\tau}} \tag{4}$$

$$0 = -ne\mathbf{E} - \nabla p_e - nm_e \left[\nu_{ei} \left(\mathbf{u}_e - \mathbf{u}_i \right) + \nu_{en} \mathbf{u}_e \right], \quad \mathbf{u}_e >> \mathbf{u}_n \tag{5}$$

$$\nabla\cdot\left(\mathbf{j}_e+\mathbf{j}_i\right)=0\rightarrow\nabla\cdot\left[\frac{\nabla\phi}{\eta}-\frac{\nabla p_e}{\eta en}-\mathbf{j}_i\left(1-\frac{\nu_{ei}}{\nu_{en}+\nu_{ei}}\right)\right]=0 \tag{6}$$

$$\frac{3}{2}\frac{\partial p_e}{\partial t}-\nabla\cdot\left(\frac{5}{2}T_e\mathbf{j}_e+\kappa_e\nabla T_e\right)=Q_e^R+Q_e^T-\mathbf{j}_e\cdot\frac{\nabla p_e}{en}-\dot{n}e\varepsilon_{ip} \tag{7}$$

$$\frac{3}{2}\frac{\partial p_{i,n}}{\partial t}+\nabla\cdot\left(\frac{5}{2}p_{i,n}\mathbf{u}_{i,n}-\kappa_{i,n}\nabla T_{i,n}\right)=Q_{i,n}^R+Q_{i,n}^T+\mathbf{u}_{i,n}\cdot\nabla p_{i,n} \tag{8}$$

All relevant elastic and inelastic collision frequencies are included in the transport terms. We have argued in the past that the resistivity η must include an "anomalous" contribution due to the presence of ion acoustic turbulence (IAT) [6, 9]. In OrCa2D this is done by assuming a linear dependence of the resistivity to an anomalous collision frequency ν_α as follows:

$$\eta=\frac{m_e\left(\nu_{en}+\nu_{ei}+\nu_\alpha\right)}{ne^2}, \tag{9}$$

where ν_{ei} and ν_{en} are the (classical) electron-ion and electron-neutral collision frequencies, respectively. The collision frequency ν_α is specified according to Sagdeev's [20] well-known formula

$$\nu_\alpha=\alpha\omega_{pi}M_e\sim\omega_{pi}\frac{u_e}{C_s}, \tag{10}$$

where the ratio of T_e/T_i in the original formula has been assumed here to be constant, and has been included in the coefficient α. This coefficient is determined in OrCa2D by iteration until the measured discharge voltage is attained by the simulation. The electron mach number M_e is defined as the ratio of the electron drift speed u_e over the thermal speed $(2kT_e/m_e)^{1/2}$. The ion acoustic speed is denoted by $C_s=(kT_e/m_i)^{1/2}$ and the ion plasma frequency is ω_{pi}.

C. **Boundary Conditions**

The emitted electron current density $\mathbf{j}_e^{em}$ from the emitter wall is specified according to the Richardson-Dushman equation for thermionic emission [21]:

$$\mathbf{j}_e^{em}\cdot\hat{\mathbf{n}}=\alpha T_w{}^2\exp\left[-\frac{e\left(\varphi_{WF}-\varphi_{SH}\right)}{kT_w}\right], \tag{11}$$

In Eq. (11) the LaB_6 emitter temperature T_w and work function φ_{WF} are implemented in the model as follows:

$$T_w\equiv T_w^0+c_1L_{em}\left(\bar{z}-1\right)+c_2L_{em}{}^2\left(\bar{z}^2-1\right)+c_3L_{em}{}^3\left(\bar{z}^3-1\right)+c_4L_{em}{}^4\left(\bar{z}^4-1\right) \tag{12}$$

$$\varphi_{WF}\equiv 2.67\,V$$

where $\bar{z}\equiv z/L_{em}$ with the length of the emitter denoted by L_{em} and c_1,c_2,c_3,c_4 are constants. The emitter

temperature profile was measured in the laboratory, as shown in Fig. 3, during operation of the cathode so the four constants "c" have been specified to match this profile. The measurements were performed with a laboratory model cathode [22] using a combination of thermocouple and fiber optic probe techniques. In this case, holes aligned with each other in the radial direction were drilled through the keeper electrode and the cathode tube to accommodate a Type C W-Re thermocouple assembly. The thermocouple was inserted through these holes and between two heater coils into a 1.5 mm diameter, 1.5 mm deep well in the LaB_6 cathode insert. Its location was approximately midway between the orifice entrance and the upstream tip of the emitter. The active junction of the thermocouple was located approximately 1.5 mm from the inner emitting surface of the insert. Thermal modeling indicates that the temperature in this location is within 10°C of the emitter temperature. This approach yielded a temperature of 1630°C at 100 A and was verified by repeated attempts. The uncertainty of ±16°C in this value is based on the thermocouple measurement uncertainty of 1% .

A fiber optic probe-based pyrometric temperature measurement system described in Ref. [23] was used to measure the temperature profile along the axis of the cathode. The thermocouple measurement in the center of the cathode was used to anchor the profile measurements. The uncertainty in the profile measurements is approximately ±20°C, which includes the uncertainty in the thermocouple measurement and uncertainties in the calibration process.

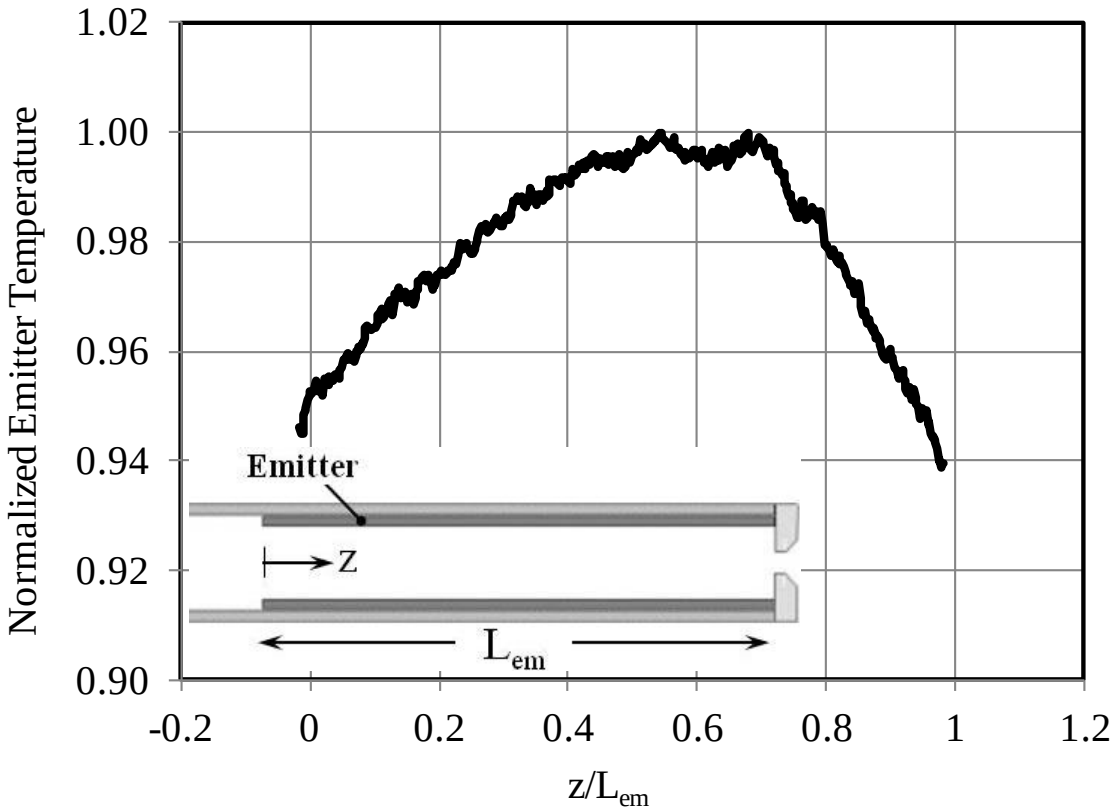

Fig. 3. Variation of the measured temperature along the LaB_6 emitter in the hollow cathode operating at 100A and 12 sccm. The profile has been used directly to specify the emitter temperature BC for the OrCa2D simulations.

In the simulations presented in this paper the temperature at the emitter tip closest to the orifice plate T_w^0 has been varied until the value of the total current through the orifice matches the operating current of the

case under investigation. The plasma potential measurements in the cathode interior have also been used to guide T_w^0. We found that that in the simulations the maximum emitter temperature had to be 36°C hotter than the measured value of 1630°C (±20°C) in order to obtain the best agreement between simulation and measurement for the plasma potential. This corresponds approximately to only ~2% change of the work function. Such changes in the material properties of the emitter are not uncommon, especially when the cathode is operated in different environments. We note that the emitter temperature measurements and the plasma measurements were performed at different times and in different vacuum chambers.

The field-enhanced emission due to the Schottky effect is included through φ_{SH} as derived in [12]. The value of φ_{WF} is taken from Ref. [24] and is based on measurements of the zero-field saturated current density obtained at various temperatures. Because φ_{SH} requires knowledge of the electric field at the wall E_w (Eq. (13)), the sheath equations in the presence of ions, plasma electrons and emitted electrons must be solved simultaneously with the plasma fluid equations. The original model for φ_{SH} has been upgraded in this latest version of OrCa2D to solve iteratively for the maximum current density that can be emitted from the insert, and the corresponding mach number of ions in the sheath, in the space charge limit where $E_w<0$. The upgrades have been based on the formulations of Prewett and Allen for the sheath conditions in the presence of electron emission [25]. This requires an iterative solution to a transcendental equation which is performed in OrCa2D using a bisection method.

$$\varphi_{SH} = \left(\frac{e|E_w|}{4\pi\varepsilon_0} \right)^{1/2} \tag{13}$$

Net emission is determined not only by the emission current density but also by the current density of electrons that are absorbed by the emitter wall, which we also account for in OrCa2D as described in Ref. [5, 12]. Ion collection at the conducting boundaries is performed in a manner that accounts for the full range of the plasma potential relative to the boundary voltage, i.e. collection in both an ion-attracting and an ion-repelling sheath. This BC for the ions was described in detail in Ref. [15] and was based on the formulations of Andrews and Varey [26].

The orifice plate temperature is set equal to the peak emitter temperature. The keeper plate temperature is set at 500 ^oC. Although this temperature may deviate from the assumed value during cathode operation the plasma results have not been found to be critically sensitive to this BC. At the anode, current is collected based on a specification of the measured discharge current. Ions that strike the anode are assumed to get neutralized and return back to the computational region as neutrals. In the experiments a cylindrical anode configuration was used that was in close proximity to the cathode. Therefore a sensitivity simulation has been performed to show the significance of neutrals returning back to the plasma in the near plume region. This is discussed further in the next section.

III. Numerical Simulations of the 100-A LaB_6 Cathode

A schematic of the cathode-anode arrangement simulated with OrCa2D is shown in Fig. 4-top. As outlined by the red dashed line, the computational region encompassed the cathode interior including the cathode plate and keeper orifices, and the plume region. The latter extended approximately 12 keeper radii downstream of the keeper orifice exit and included the cylindrical anode as shown also in the experimental setup in Fig. 4-bottom. The coordinate system used here is an axisymmetric system with the r-z origin located at the intersection of the cathode centerline and the entrance to the cathode orifice as shown in the top corner of Fig. 4-top. The operating conditions for all simulations presented herein was 100 A and 12 sccm of xenon. The experimental arrangement and diagnostics for the plasma measurements have been described in detail in Ref. [22].

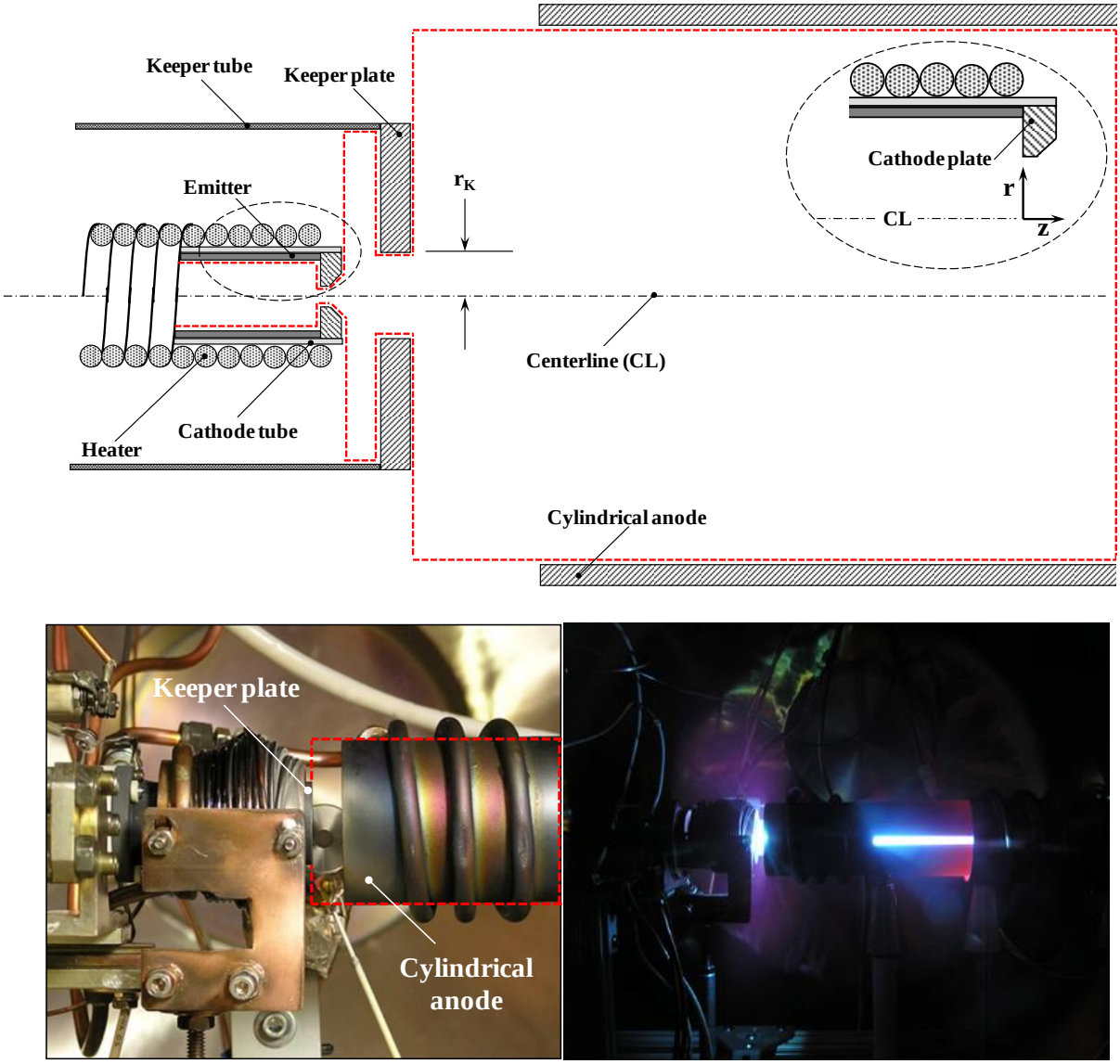

Fig. 4. The hollow cathode and anode arrangement as used in both the numerical simulations and the laboratory experiments. Top: Schematic showing critical components. The computational region for the simulations is depicted by the red dashed outline. Bottom-left: The experimental setup showing the cylindrical anode location relative to the keeper plate. The red dashed outline points to the extent of the computational region in the cathode plume (also termed the anode region in this paper) as used in the simulations. Bottom-right: The LaB_6 hollow cathode operating in a vacuum facility.

Since this is the first time a simulation of a LaB_6 cathode operating at high discharge currents has been performed we found it constructive to compare the plasma conditions in this cathode with those in a more well-known cathode environment. We have chosen to make the comparison with the NASA Solar Electric Propulsion Technology Application Readiness (NSTAR) discharge hollow cathode (DHC) since this device had been studied extensively both by analyses [6, 14, 16, 27] and experiments [7, 10]. A comparison of the LaB_6 hollow cathode operating at 100 A and 12 sccm with the NSTAR DHC operating at 13.3 A and 3.7 sccm is shown in Fig. 5. It is noted that the emitter diameter in the LaB_6 cathode is approximately 2.5× larger than that in the NSTAR DHC, and the cathode orifice diameter is 4.725× larger. A comparison of the two geometries is shown in Fig. 5-left. As a result the maximum electron

current density, which occurs in the orifice, is in fact ~4.2× higher in the NSTAR DHC than in the LaB_6 cathode (2000 A/cm^2 vs. 480 A/cm^2). Similarly, although the characteristic size of the interior plasma is larger in the LaB_6 cathode due in part to its larger dimensions, the peak plasma density achieved inside the cathode is in fact lower than that in the NSTAR DHC. This can be seen clearly by the comparison of the computed electron number densities in the 2-D contour plots of Fig. 5-left and along the cathode centerline in Fig. 5-right. The higher number densities in the plume region of the LaB_6 cathode are due to the size and proximity of the cylindrical anode to the cathode which leads to a significant contribution of neutrals to the near-plume. It is noted that the results of these simulations for the LaB_6 cathode did not account for the inertia (left-hand-side) terms in the ion momentum equation (Eq. (3)), to allow for a one-on-one comparison with NSTAR results which also assumed ion diffusion only.

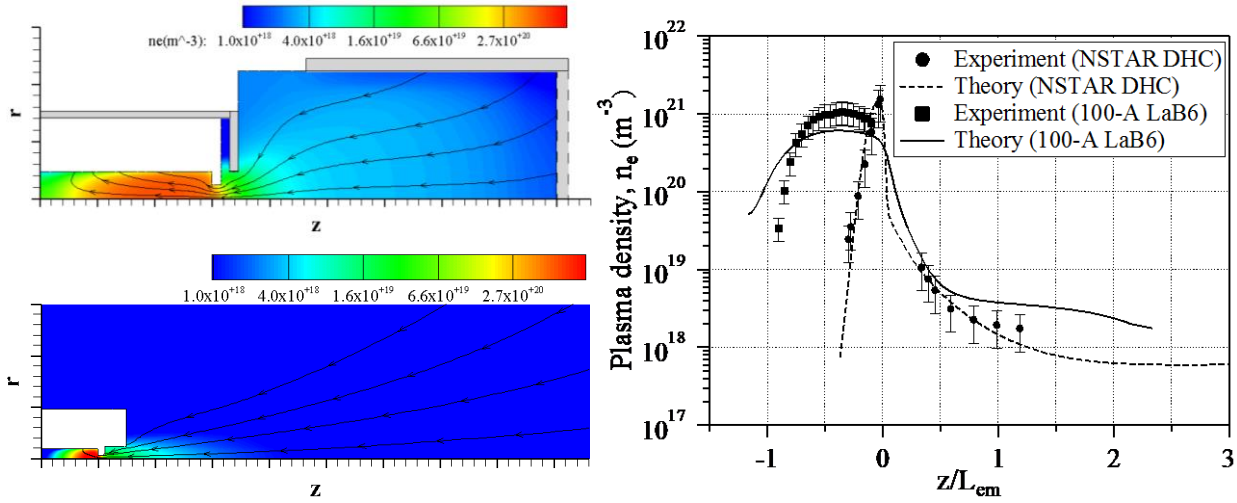

Fig. 5. Comparison of the LaB_6 hollow cathode operating at 100 A and 12 sccm with the NSTAR DHC operating at 13.3 A and 3.7 sccm. Left: Simulation results for the electron number density showing the significantly different geometries of the two cathodes. Also shown are representative electron current density streamlines. Right: Comparison of the electron number densities along the centerline of the two cathodes.

The enhancement of the electron number density in the cathode plume was seen clearly by the results of a sensitivity simulation, performed to quantify the effects of neutral contributions to the plume due to the presence of the cylindrical anode. The simulations compared the fiducial case in which all ion flux to the anode boundary was returned back to the plume as neutrals (Fig. 6-left-top), and a test case in which all ions were assumed to be fully absorbed by the anode (Fig. 6-left-bottom). Both simulations were conducted assuming no ion inertia in the momentum equation (Eq. (3)). Because the computational region cannot be extended to include the full length of the anode used in the experiment, an anode boundary was assumed at the downstream vertical boundary of the computational region. This is represented by the dashed rectangle Fig. 6-left-top. The second case is more akin to the NSTAR DHC operation where the anode is much farther away from the cathode. The electron number density along the cathode centerline for the two cases is compared in Fig. 6-right. We find the contribution to the plume density due to the presence of neutrals from the anode to exceed one order of magnitude in the far plume regions of the computational region. It is noted that all simulations have assumed the anode is at room temperature. At the high discharge currents considered here the anode can become hot enough to glow in which case the contribution of neutrals would be less.

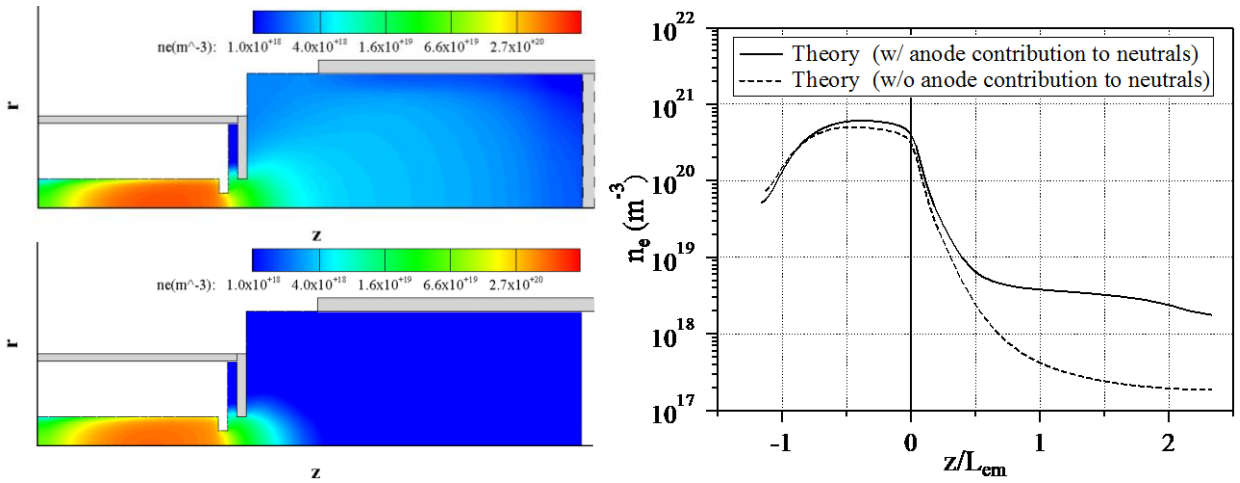

Fig. 6. Effects of cylindrical anode on the cathode plume. The simulations results shown here have been produced without the ion inertia terms (Theory-1 model). Left: Electron number density contours assuming (top) ions are neutralized at the anode and return to the plume as neutrals and (bottom) ions are fully absorbed by the anode. Right: Computed electron number density along the cathode centerline comparing the two aforementioned cases.

Although the assumption of ion-diffusion dominated plasma in the cathode interior may be valid, it has long been speculated that ion inertia effects may become important in the cathode plume. The argument *for* the importance of the ion inertia has its roots in experimental evidence that ions with energies far exceeding the discharge voltage can persist in the near plume region [22]. For example recent measurements in the near plume of the LaB_6 cathode studied here showed ion energies that exceeded 100 V during operation at 100 A. We proposed in the past that the source of such energetic ions could be free energy from streaming instabilities that can be excited in the cathode near plume where the electron Mach number has been found to approach or exceed unity and the collisions of electrons with other particles become rare [6, 9]. We therefore extended OrCa2D to include the ion inertia terms as shown in Eq. (3), and performed a simulation at the same operating condition the results of which are shown in Fig. 7-right. The computed electron number density contours are compared with those from the ion-diffusion model in Fig. 7-left. For brevity, to distinguish the two solutions we have termed the ion-diffusion model "Theory-1" and the model with the inertia terms "Theory-2". All results presented prior to the ones on Fig. 7-right have been with the Theory-1 model. The contour plots show clearly that the effects of ion inertia become non-negligible only along the keeper region. This is better quantified in Fig. 8 showing plots of plasma variables along the cathode centerline (left), and along the keeper electrode (right) approximately $0.04r_K$ downstream of the surface facing the anode. The comparison on Fig. 8-left shows only minor differences between the two models along the cathode centerline. Contrary to our previous simulations of the NSTAR DHC (e.g. see [16]), we found that the LaB_6 simulation under-predicts the measured electron number density in the cathode interior by about a factor of 1.7×. The comparison for the plasma potential and electron temperature shows the simulation results to be within the experimental uncertainty for most of the cathode interior. Though not yet proven, the discrepancy in the electron number density may be associated with minor differences in the emitter temperature profile implemented as the BC. Sensitivity simulations at a lower discharge current have shown that the steady-state profile of the interior plasma is quite sensitive to small changes in the variation of the temperature along the emitter. Such sensitivity simulations for the 100-A case are ongoing.

The largest impact of the ion inertia terms is found to be in the radial expansion of the plasma near the keeper. Due to the acceleration of the ions in this region we found that the plasma density is as much as 5× lower in the model that accounts for ion inertia, as plotted in Fig. 8-right. Smaller differences between the two models were found for the plasma potential and electron temperature as shown in Fig. 8-right.

This steady-state acceleration though leads to ion energies in this region that do not exceed a few volts, so the additional terms in Eq. (3) are not sufficient to explain the presence of measured [22] energetic ions.

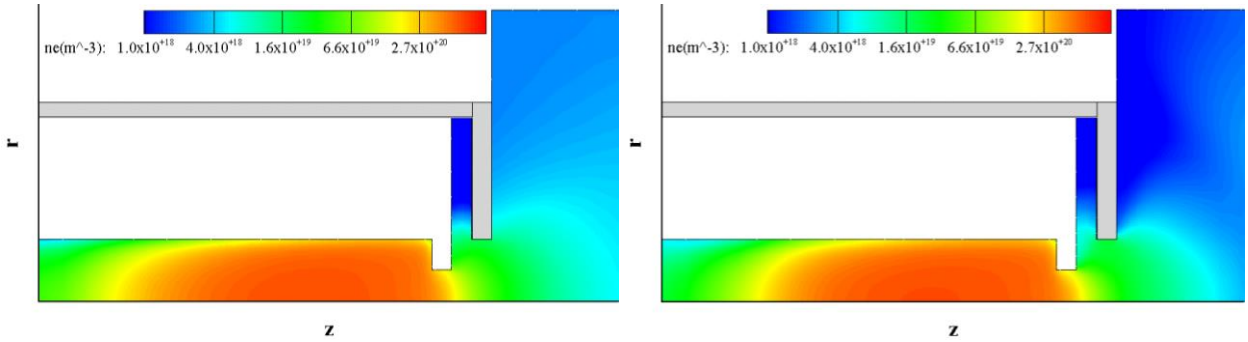

Fig. 7. Comparison of the computed electron number density without accounting for the ion inertia (left) and with the inertia terms (right). In this article, the inertia-less or diffusion model is termed "Theory-1" and the model with the inertia terms is called "Theory-2." The Theory-2 model yields in the vicinity of the keeper steady-state ion energies that do not exceed a few volts.

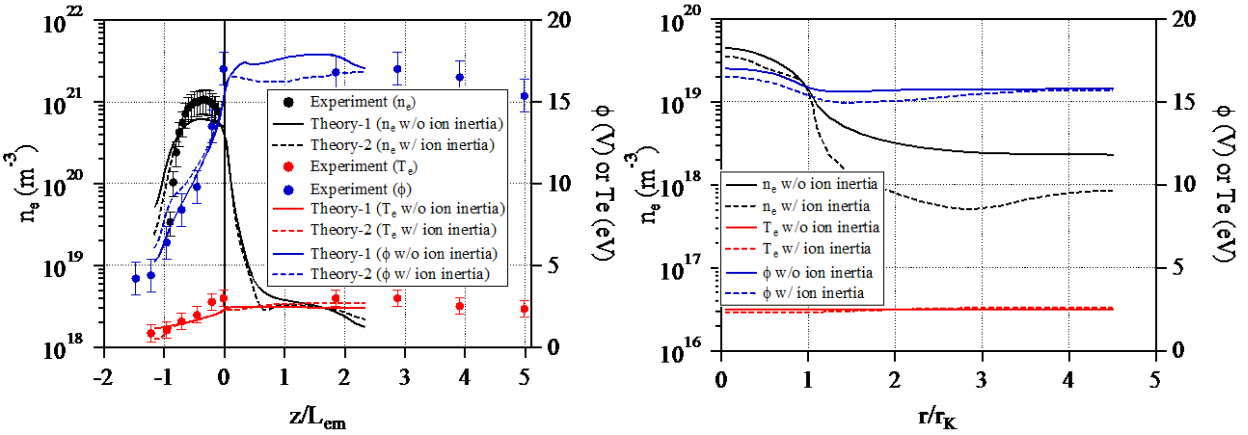

Fig. 8. Comparison of the electron number density, plasma potential and electron temperature along the centerline (left) and along the keeper electrode of the LaB_6 hollow cathode operating at 100 A and 12 sccm.

We have argued in the past that if the source of the high-energy ions is streaming instabilities, such effects would not be captured by the fluid model of OrCa2D due to the kinetic nature of these instabilities. As with the simulations of the smaller cathodes, like the NSTAR DHC, we found in the simulations of the 100-A LaB_6 cathode evidence that streaming instabilities that can lead to IAT could get excited here as well. In Fig. 9-top-left we plot contours of the electron Mach number in the vicinity of the cathode plate and keeper electrodes. The results were computed with the Theory-2 model. As in previous cathodes [6, 9] we found here that the Mach number can approach and even exceed unity along the keeper face, where electron collisions also become rare. This suggests a region where ion-acoustic waves can become unstable leading to IAT. The plot on Fig. 9-bottom-left compares ν_{ei} and ν_{en} with the (IAT) anomalous collision frequency (ν_α) implemented in OrCa2D according to Eq. (10). It can be seen that ν_α is as much as ~4× higher than the sum of the two classical collision frequencies in this region. An experimental effort that has focused on identifying the turbulent spectra in this cathode has been performed in parallel to the numerical simulations reported in this article. This effort has confirmed the presence of IAT in the cathode plume, and yielded an effective collision frequency that is comparable to

the values predicted by the numerical simulations. The computed anomalous collision frequency ν_α at 12 sccm, using the two models used in these simulations is plotted along the cathode CL in Fig. 9-bottom-right. Also shown is the measured value of ~4×10^8 s^{-1} at 10 sccm. A measurement at 12 sccm and 100 A was not performed but at 15 sccm and 110 A the value dropped to ~0.15×10^8 s^{-1} due to damping by ion-neutral collisions. The results of the experimental effort are reported in our companion paper [13]. At the location of the measurement the two OrCa2D models Theory-1 and Theory-2 yield 1.6×10^8 s^{-1} and 0.5×10^8 s^{-1}, respectively. Also in accordance to our previous simulation results in smaller cathodes, we found a similar structure of the plasma potential in the keeper region. Specifically, albeit small, we found that a sufficient gradient of the potential is established that, combined with the sheath, turns ions towards the keeper face. This is shown by the unit vectors of the Xe^+ ion flux in Fig. 9-top-right. In light of the high-energy ions measured in the laboratory, the plasma turbulence predicted to exist by the simulations and confirmed by recent experiments, and the direction of the steady-state ion flux, it is argued that erosion of the keeper electrode will proceed unimpeded in this cathode.

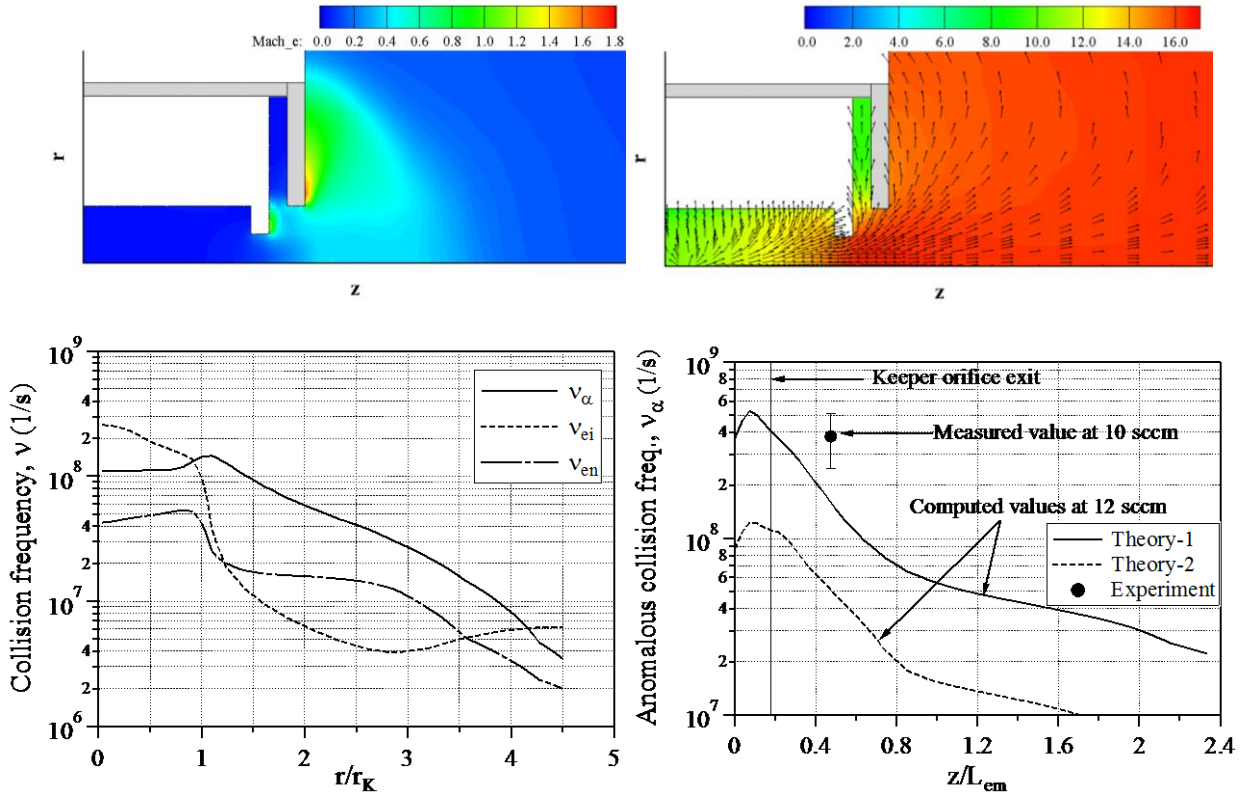

Fig. 9. Top-left: Contours of electron Mach number in the vicinity of the orifice plate and keeper electrodes. Top-right: Contours of plasma potential overlaid by unit vectors of Xe^+ ion flux. Bottom-left: Comparison of the electron collision frequencies along a radial slice that is approximately $0.04r_K$ downstream the keeper electrode surface facing the anode. Bottom-right: The computed ν_α along the cathode CL at 12 sccm. Also shown is the measured value of ~4×10^8 s^{-1} at 10 sccm. A measurement at 12 sccm and 100 A was not performed but at 15 sccm and 110 A the value dropped to ~0.15×10^8 s^{-1} (largely due to damping by ion-neutral collisions) [13].

IV. Conclusions

After the recent breakthrough advances on channel erosion enabled by magnetic shielding, the last known major life-limiting mechanism that remains unsolved in high-power Hall thrusters is erosion of the keeper electrode in the hollow cathode. High-power Hall thrusters will require cathodes that operate at discharge currents in the range of 50-250 A, which is more than one order of magnitude higher than state-of-the-art cathodes such as the NSTAR DHC. Though operation of cathodes at these discharge currents has remained relatively unexplored, it is known that anomalously large ion energies can be produced that, in some cases, can exceed 100 V. Such energies are sufficient to cause erosion of the keeper at rates that are much higher than those needed for human and robotic exploration missions envisioned by NASA, like ARM. Though several hypotheses have been made in the last few decades, the source of these high-energy ions has remained elusive. A 2-year research effort began at JPL in 2013 with the objective to identify the source(s) of these high energy ions using a combination of numerical simulation and experiments. This paper has presented results from the first numerical simulations of a LaB6 hollow cathode operating at 100 A and 12 sccm of xenon flow, without an applied magnetic field. The objective of these first series of simulations has been to establish the steady-state plasma conditions upon which further numerical and experimental investigations can be pursued that will focus on the link between plasma oscillations and high energy ions.

Operation at 100 A is not found to lead to plasma conditions in the LaB_6 cathode interior that are atypical compared to their smaller counterparts operating at much lower discharge currents. Temperatures along the LaB_6 emitter appear to be in the range of ~1600 ^{o}C which should not lead to prohibitive limitations related to the emitter life. The maximum electron current densities occur as expected in the cathode orifice, and are significantly lower than the values found in the NSTAR DHC which exhibited no erosion of the orifice plate after tens of thousands of hours of testing. The lower resistive drops across the orifice that are therefore seen in the LaB_6 cathode are not expected to lead to any erosion of the orifice plate. Thus, the only concern remains erosion of the keeper which is expected to occur at high rates due to the known presence of ions with energies that far exceed the discharge voltage. As in the smaller cathodes, the numerical simulations of the LaB_6 cathode at 100 A suggest that the conditions for the excitement of current-driven streaming instabilities are satisfied, especially along the keeper electrode where erosion occurs. In this region we find that the IAT-driven anomalous resistivity is as much as ~4× higher than the sum of the two classical collision frequencies in this region. In a parallel experimental effort aimed at measuring the dominant wave spectra, the presence of IAT has been confirmed and the measured anomalous collision frequency agrees well with the predictions of the fluid numerical simulations. The results of the experimental effort are reported in a companion paper [13].

Acknowledgments

The research described in this paper was carried out by the Jet Propulsion Laboratory, California Institute of Technology, under a contract with the National Aeronautics and Space Administration and funded through the internal Research and Technology Development program. The authors wish to acknowledge Olga S. Filimonova for providing a large portion of the time-averaged plasma measurements in the LaB6 hollow cathode.

References

[1] I.G. Mikellides, I. Katz, R.R. Hofer, D.M. Goebel, K. de Grys, A. Mathers, Magnetic shielding of the channel walls in a Hall plasma accelerator, Physics of Plasmas, 18 (2011) 033501.
[2] I.G. Mikellides, I. Katz, R.R. Hofer, D.M. Goebel, Magnetic shielding of walls from the unmagnetized ion beam in a Hall thruster, Appl Phys Lett, 102 (2013).
[3] T. Jones, The View From Here: Snaring a Piece of the Sky, in: Aerospace Am, American Institute of Aeronautics and Astronautics, Reston, VA, 2012, pp. 2.

[4] J. Brophy, C. Garner, AIAA Paper No. 88-2193, in: 24th AIAA/ASME/SAE/ASEE Joint Propulsion Conference, Boston, MA., American Institute of Aeronautics and Astronautics, Washington, DC, 1988, pp. 2193.
[5] L.G. Mikellides, I. Katz, Wear mechanisms in electron sources for ion propulsion, 1: Neutralizer hollow cathode, J Propul Power, 24 (2008) 855-865.
[6] I.G. Mikellides, I. Katz, D.A. Goebel, K.K. Jameson, J.E. Polk, Wear mechanisms in electron sources for ion propulsion, 2: Discharge hollow cathode, J Propul Power, 24 (2008) 866-879.
[7] D.M. Goebel, J.E. Polk, I.G. Mikellides, Ion Thruster Performance Impacts due to Cathode Wear, J Propul Power, 27 (2011) 768-776.
[8] D.M. Goebel, K.K. Jameson, R.M. Watkins, I. Katz, I.G. Mikellides, Hollow cathode theory and experiment. I. Plasma characterization using fast miniature scanning probes, J Appl Phys, 98 (2005).
[9] I.G. Mikellides, I. Katz, D.M. Goebel, K.K. Jameson, Evidence of nonclassical plasma transport in hollow cathodes for electric propulsion, J Appl Phys, 101 (2007).
[10] D.M. Goebel, K.K. Jameson, I. Katz, I.G. Mikellides, Potential fluctuations and energetic ion production in hollow cathode discharges, Physics of Plasmas, 14 (2007).
[11] I.G. Mikellides, I. Katz, D.M. Goebel, J.E. Polk, AIAA Paper 04-3817, in: 40th AIAA/ASME/SAE/ASEE Joint Propulsion Conference, Fort Lauderdale, FL, American Institute of Aeronautics and Astronautics, Washington, DC, 2004, pp. 3817.
[12] I.G. Mikellides, I. Katz, D.M. Goebel, J.E. Polk, Hollow cathode theory and experiment. II. A two-dimensional theoretical model of the emitter region, J Appl Phys, 98 (2005).
[13] B.A. Jorns, I.G. Mikellides, D.M. Goebel, IEPC Paper No. 13-385, in: 33rd International Electric Propulsion Conference (IEPC Paper No. 13-385), Washington, DC, Electric Rocket Propulsion Society, Fairview Park, OH, 2013.
[14] I.G. Mikellides, I. Katz, D.M. Goebel, J.E. Polk, K.K. Jameson, Plasma processes inside dispenser hollow cathodes, Physics of Plasmas, 13 (2006).
[15] I.G. Mikellides, D.M. Goebel, J.S. Snyder, I. Katz, D.A. Herman, The discharge plasma in ion engine neutralizers: Numerical simulations and comparisons with laboratory data, J Appl Phys, 108 (2010).
[16] I.G. Mikellides, Effects of viscosity in a partially ionized channel flow with thermionic emission, Physics of Plasmas, 16 (2009).
[17] S.K. Godunov, A Difference Method for the Numerical Calculation of Discontinuous Solutions of Hydrodynamic Equations, Math. Sbornik, 47 (1959) 271-306.
[18] I. Katz, I.G. Mikellides, Neutral gas free molecular flow algorithm including ionization and walls for use in plasma simulations, J Comput Phys, 230 (2011) 1454-1464.
[19] I.G. Mikellides, I. Katz, Numerical simulations of Hall-effect plasma accelerators on a magnetic-field-aligned mesh, Physical Review E, 86 (2012) 046703.
[20] R.Z. Sagdeev, A. Galeev, Nonlinear plasma theory, W. A. Benjamin, New York,, 1969.
[21] S. Dushman, Electron emission from metals as a function of temperature, Phys Rev, 21 (1923) 0623-0636.
[22] E. Chu, D.M. Goebel, High-Current Lanthanum Hexaboride Hollow Cathode for 10-to-50-kW Hall Thrusters, Ieee T Plasma Sci, 40 (2012) 2133-2144.
[23] J.E. Polk, C.M. Marrese-Reading, B. Thornber, L. Dang, L.K. Johnson, I. Katz, Scanning optical pyrometer for measuring temperatures in hollow cathodes, Rev Sci Instrum, 78 (2007).
[24] E.K. Storms, B.A. Mueller, Study of Surface Stoichiometry and Thermionic Emission Using Lab, J Appl Phys, 50 (1979) 3691-3698.
[25] P.D. Prewett, J.E. Allen, Double Sheath Associated with a Hot Cathode, Proc R Soc Lon Ser-A, 348 (1976) 435-446.
[26] J.G. Andrews, R.H. Varey, Sheath at an Electrode Close to Plasma Potential, Journal of Physics, A: General Physics, 3 (1970) 413-420.
[27] I. Katz, I.G. Mikellides, J.E. Polk, D.M. Goebel, S.E. Hornbeck, Thermal model of the hollow cathode using numerically simulated plasma fluxes, J Propul Power, 23 (2007) 522-527.